Experimental Neurology 254 (2014) 109–120

Contents lists available at ScienceDirect

Experimental Neurology

journal homepage: www.elsevier.com/locate/yexnr

High-resolution intravital imaging reveals that blood-derived macrophages but not resident microglia facilitate secondary axonal dieback in traumatic spinal cord injury ☆

Teresa A. Evans [a], Deborah S. Barkauskas [b,c], Jay T. Myers [c], Elisabeth G. Hare [a], Jing Qiang You [a], Richard M. Ransohoff [d], Alex Y. Huang [c,*], Jerry Silver [a,**]

[a] Department of Neurosciences, Case Western Reserve University School of Medicine, Cleveland, OH 44106, USA
[b] Department of Biomedical Engineering, Case Western Reserve University School of Medicine, Cleveland, OH 44106, USA
[c] Department of Pediatrics, Case Western Reserve University School of Medicine, Cleveland, OH 44106, USA
[d] Department of Neurosciences, Neuroinflammation Research Center, Lerner Research Institute, Cleveland Clinic Foundation, Cleveland, OH 44195, USA

ARTICLE INFO

Article history:
Received 10 October 2013
Revised 12 December 2013
Accepted 11 January 2014
Available online 24 January 2014

Keywords:
Spinal cord injury
Two-photon microscopy
Microglia
Monocytes
Macrophages
Bone marrow chimera mice
Axonal dieback
Retraction bulb
CX3CR1
CCR2

ABSTRACT

After traumatic spinal cord injury, functional deficits increase as axons die back from the center of the lesion and the glial scar forms. Axonal dieback occurs in two phases: an initial axon intrinsic stage that occurs over the first several hours and a secondary phase which takes place over the first few weeks after injury. Here, we examine the secondary phase, which is marked by infiltration of macrophages. Using powerful time-lapse multi-photon imaging, we captured images of interactions between *Cx3cr1*$^{+/GFP}$ macrophages and microglia and *Thy-1*^{YFP} axons in a mouse dorsal column crush spinal cord injury model. Over the first few weeks after injury, axonal retraction bulbs within the lesion are static except when axonal fragments are lost by a blebbing mechanism in response to physical contact followed by phagocytosis by mobile *Cx3Cr1*$^{+/GFP}$ cells. Utilizing a radiation chimera model to distinguish marrow-derived cells from radio-resistant CNS-resident microglia, we determined that the vast majority of accumulated cells in the lesion are derived from the blood and only these are associated with axonal damage. Interestingly, CNS-resident *Cx3Cr1*$^{+/GFP}$ microglia did not increasingly accumulate nor participate in neuronal destruction in the lesion during this time period. Additionally, we found that the blood-derived cells consisted mainly of singly labeled *Ccr2*$^{+/RFP}$ macrophages, singly labeled *Cx3Cr1*$^{+/GFP}$ macrophages and a small population of double-labeled cells. Since all axon destructive events were seen in contact with a *Cx3Cr1*$^{+/GFP}$ cell, we infer that the CCR2 single positive subset is likely not robustly involved in axonal dieback. Finally, in our model, deletion of CCR2, a chemokine receptor, did not alter the position of axons after dieback. Understanding the *in vivo* cellular interactions involved in secondary axonal injury may lead to clinical treatment candidates involving modulation of destructive infiltrating blood monocytes.

Introduction

Axons severed by traumatic injury not only fail to regrow but retract from the center of the lesion over the first few weeks after injury. Retracting axonal endings form a variety of unusually shaped tips (Busch et al., 2009; Kerschensteiner et al., 2005) which Ramon y Cajal described as retraction clubs, linking their anatomy to their unusual dying back behavior (Cajal, 1907). Over the first few hours after injury, the early phase of retraction occurs by a neuron intrinsic mechanism with axonal beading and rapid dissolution of the distal axon segment (Kerschensteiner et al., 2005). In the subsequent days and weeks following injury a less well described secondary period of dieback occurs which is correlated with infiltration of blood-derived immune cells, including macrophages (Busch et al., 2009; Fitch and Silver, 2008). The role of these macrophages in the lesion has been controversial, with evidence that these cells are both beneficial (Schwartz and Yoles, 2006; Shechter et al., 2009, 2013) as well as destructive (Busch et al., 2009; Donnelly and Popovich, 2008; Fitch and Silver, 2008; Hsu et al., 2006; Popovich et al., 1999).

It is well known that the secondary period of dieback can be influenced by depleting circulating phagocytic cells, including macrophages

Abbreviations: DCC, dorsal column crush.
☆ The authors declare no competing financial interests.
* Correspondence to: A.Y. Huang, WRB 6528, 2103 Cornell Road, Cleveland, OH 44106-7288, USA. Fax: +1 216 368 0741.
** Correspondence to: J. Silver, 2109 Adelbert Road, Cleveland, OH 44106, USA. Fax: +1 216 368 4650.
E-mail addresses: teresa.evans@case.edu (T.A. Evans), deborah.sim@case.edu (D.S. Barkauskas), jay.myers@case.edu (J.T. Myers), ehare@laurelschool.org (E.G. Hare), jxy268@case.edu (J.Q. You), ransohr@ccf.org (R.M. Ransohoff), ayh3@case.edu (A.Y. Huang), jxs10@case.edu (J. Silver).

http://dx.doi.org/10.1016/j.expneurol.2014.01.013

via the use of Clodronate liposomes which, when taken up by phagocytic cells, cause their death by apoptosis (Van Rooijen and Sanders, 1994). In macrophage depleted animals, there was no further change in axonal position beyond that which occurred initially, strongly implicating macrophages in the delayed dieback phenomenon (Horn et al., 2008). Decrease in dieback has also been shown in minocycline treated rats with a reduced macrophage response (McPhail et al., 2004). The destructive interaction between inflammatory cells and dystrophic axons was further corroborated by *in vitro* studies showing that activated macrophages can cause striking retraction of dystrophic axons in a contact-dependent manner, while cultured microglia had a lesser effect (Busch et al., 2009). In culture, axonal retraction after contact with activated macrophages could be inhibited by functionally blocking MMP9 but not MMP2 (Busch et al., 2009). Although much is known about the requirement for macrophages in this phenomenon, very little is known about how these cells actually interact *in vivo*.

The population of phagocytic immune cells found in the CNS is heterogeneous and comprised predominantly of two groups: specialized CNS-resident microglia and infiltrating macrophages. Microglial cells arrive in the CNS from the yolk sack in development (Ginhoux et al., 2010; Kierdorf et al., 2013b), renew by local proliferation (Ajami et al., 2007), are responsible for surveying the CNS parenchyma (Nimmerjahn et al., 2005) and aid in synaptic pruning (Schafer et al., 2012). In injury, the microglia react immediately to damage (Davalos et al., 2005) while macrophages enter the site later in response to signals from injured tissues (Stirling and Yong, 2008). Those which induce macrophages to leave the blood vessel including CCL7, IL-1 and TNF-beta do so indirectly through enhancement of selectin expression on blood vessels (Takeshita and Ransohoff, 2012). The microglia and monocyte-derived macrophages are historically difficult to differentiate, as they express many of the same markers including ED-1, Iba-1 and CX3CR1. They can be crudely distinguished based on differing levels of CD45 or CCR2 (David and Kroner, 2011) and differential susceptibility to radiation (Matsumoto and Fujiwara, 1987).

Infiltrating macrophages can be divided into yet more subgroups: a patrolling subgroup whose cells are Ly6c^{-}, CX3CR1^{hi}, CCR2^{lo} cells and the inflammatory subset, expressing Ly6c^{+}, CX3CR1^{lo} and CCR2^{hi} (Geissmann et al., 2003). Both of these cellular subtypes are found in traumatic lesions, but their possible differential effects have not been thoroughly studied. Phagocytic immune cells traffic towards cytokines secreted from injured tissue and can enter tissues after injury by extravasation either during bleeding or by transmigration across blood vessels using selectins expressed on the surface of endothelial cells. The best known receptor ligand pairs for macrophage chemotaxis into damaged tissues include CCR2 and its ligands CCL2/CCL7, CCR1/CCR5 and their ligands CCL3/CCL5 and CX3CR1and its ligand, Fractalkine. Fractalkine signals via contact-dependent interactions as a membrane molecule and, after cleavage, at a distance. The functional roles of both CCR2 and CX3CR1 have been studied in spinal cord injury, but details about their role in secondary dieback are lacking (Corona et al., 2010; Donnelly et al., 2011; Ma et al., 2002).

In this study, we applied real-time, high-resolution, dynamic *in vivo* imaging to characterize the close interactions that occur *in vivo* between immune cells and axons during the secondary phase of axonal retraction to determine whether dieback transpires *in vivo* as it does *in vitro* (Busch et al., 2009). Using bone marrow chimeras, we show that blood-derived *Cx3cr1*$^{+/GFP}$ macrophages rather than *Cx3cr1*$^{+/GFP}$ microglia are responsible for secondary axonal damage after SCI via a contact mediated mechanism that results in thinning and breaking of the distal portion of the axon. Since all cells causing destructive events appeared to be blood derived *Cx3cr1*$^{+/GFP}$ we have identified the blood-derived monocyte subtype as the cell type primarily involved in this interaction. In this model, the axonal die back phenomenon was not dependent on the expression of functional CCR2, implicating other signaling mechanisms, including CX3CR1, for neuronal destruction by this patrolling monocyte subset.

Materials and methods

Transgenic mice

Single, double and triple transgenic mice from the *Thy-1*^{YFP} H (Feng et al., 2000), *Thy-1*^{CFP} (Feng et al., 2000), *Cx3cr1*$^{+/GFP}$ (Jung et al., 2000) and *Ccr2*$^{+/RFP}$ (Saederup et al., 2010) lines were used. All animals are on a C57BL6 background. Multiple transgenic lines included the double transgenic lines *Thy-1*$^{+/YFP}$ H × *Cx3cr1*$^{+/GFP}$ and *Thy-1*$^{+/YFP}$ H × *Cx3cr1*$^{GFP/GFP}$ and the triple transgenic lines *Thy-1*$^{+/YFP}$ H × *Cx3cr1*$^{+/GFP}$ × *Ccr2*$^{+/RFP}$ and *Thy-1*$^{+/YFP}$ H ×*Cx3cr1*$^{+/GFP}$ × *Ccr2*$^{RFP/RFP}$. We used adult mice from 8 to 20 weeks of age, with equal numbers of male and female mice. Mice were housed and bred in the animal resource center facilities at the Case Western Reserve University according to standard husbandry practices. All experiments and animal handling were performed in accordance with protocols approved by the Institutional Animal Care and Use Committee.

Chimeras

Bone marrow transplants were performed when host animals were 10–14 weeks of age. Animals were irradiated at 980 rads, and allowed to rest for 4–5 h. Hosts received 3 million donor cells isolated from the femur and tibia of donor animals by tail vein injection. Chimera efficiency was verified in the blood 10 weeks post-transplant. Chimera efficiency was established using flow cytometry of blood collected from these animals at 8–12 weeks after transplant. Details of flow cytometry experiments are found below in "Flow cytometry". Chimerism was determined by comparing the number of F4/80 and CX3CR1^{GFP} cells. Animals in which the host and the donor were the same genotype were used as a comparison. In animals with the same host and donor, an average of 40.36% CX3CR1GFP cells were found in the blood, with a low of 36.0% and a maximum of 43.6%. In animals with a CX3CR1^{GFP} host and B6 donor, the average percentage CX3CR1 positive cells found in the blood was 0.58% and ranged from 1.4% to 0.1%. In animals with a B6 host and CX3CR1^{GFP} donor, the average number of CX3CR1 positive cells found in the blood was 38.73% and ranged from 30.8% to 54.2%. The overall average efficiency of transplantation was 95.95%. Using a two-tailed *t*-test assuming two samples of unequal variance, the P value comparing transplanted animals with different host and donor to those with the same genotype host and donor was $^{*}P < 0.00001$.

Dorsal column crush (DCC) spinal injury model

Mice were anesthetized with inhaled isoflurane gas (2%) for all surgical procedures. A modified version of DCC spinal cord injury described previously (Shen et al., 2009) was performed. Briefly, a laminectomy was performed to expose the T10 spinal cord segment. Small holes were made in the dura 0.5 mm lateral to the midline with a 30 gauge needle and a DCC lesion was made by inserting Dumont # 4 jeweler's forceps approximately 1 mm into the dorsal spinal cord and squeezing, holding pressure for 10 s and repeating two additional times. The laminectomy site was covered with saline-soaked gelfoam (Pfizer) and the muscle and skin closed. The animals received Marcaine (1.0 mg/kg) subcutaneously along the incision site as well as buprenorphine (0.1 mg/kg) intramuscularly. For sham surgeries, the animals received a laminectomy and the intact dura was covered with gelfoam.

In vivo imaging of the DCC lesion with two-photon microscopy

Intravital imaging was performed 0, 2, 4, 5 and 8 days after lesion using a Leica SP5 confocal microscope fitted with a 16 W IR laser (Coherent, Inc.). To minimize artifacts from breathing and heartbeat, the spine was stabilized using a STS-A small animal spinal cord holder (Narishige International USA, Inc.) on a customized base. A well for

immersion fluid (Dulbecco's aCSF) was then formed around the spinal clamps with OrthoJet dental acrylic (Lang Dental Manufacturing Co., Inc.). Vessels were labeled by tail vein injection of TRITC-dextran (150,000 MW; Sigma). High-resolution 3D (xyz) images with a z-step size of 3 μm were taken of the top approximately 150 μm of the spinal column. For each animal, mosaic images of the entire opened portion of the spinal column were taken. Additionally, 1–6 hour-long high-resolution 4D (xyzt) movies were acquired with a frame rate of 60 s/frame at the caudal side of the lesion where retraction bulbs are found. If any evidence of thermal damage was observed, the samples were not used. This included bubbling, changes in general structure of the sample or swelling of the sample.

Flow cytometry

Five days after a DCC injury, *Cx3cr1*$^{+/GFP}$ animals were euthanized by CO_2 inhalation. Blood was collected by cardiac puncture and the spleen and spinal cord were harvested. Each group consisted of 3 male mice. 20 μl of blood was incubated with heparin, the entire spleen and the section of spinal cord including the DCC injury and 1 mm rostral and caudal to the lesion were treated with collagenase and placed on ice for 1 h. Single cell suspensions of the spleens and spinal cords were generated by pressing tissue through a 40 μm cell strainer (Corning) using the plunger from a 1 ml syringe (BD) and suspended in PBS with 5% serum (FACS buffer). Blood and tissue homogenates were red cell lysed with ACK lyse (Life Technologies) 1–3 times or until the pellet was no longer red in color, counted on a hemocytometer, and stained with PE conjugated F4/80 antibody (eBioscience) at a concentration of 1/100. Genetically expressed CX3CR1^{GFP} was used to identify CX3CR1 + cells. CD11b PE and CX3CR1^{GFP} served as positive controls for color compensation and an isotype control was also used for F4/80 (eBioscience). Samples were analyzed on an Accuri flow cytometer (BD Biosciences) using default flow parameters. Analysis was performed using CFlow Plus (BD Biosciences).

Sciatic nerve PhRodo injection

Animals received an injection of PhRodo-conjugated dextran 10,000 MW (Invitrogen) unilaterally into the sciatic nerve 6 days after a DCC injury. Briefly, the sciatic nerve of the right hind limb was exposed and crushed with #4 forceps. A 4–0 prolene suture was placed around the nerve distal to the crush site, and a hole formed in the epineurium distal to the suture with a 30-gauge needle through which a Hamilton syringe was inserted and 1 μl of PhRodo-dextran (10% in water) was injected into the crush site. Only animals where the crush site was successfully filled with dye were used for the experiments. The suture was tightened enough to prevent immediate backflow of dye through the hole, but was not secured tightly around the nerve to avoid ligation of the nerve and the animal was sutured closed. Animals received sub cutaneous Marcaine (1.0 mg/kg) and intramuscular bupernex (0.1 mg/kg) (Butler Schein). Animals were imaged as described previously two days after sciatic nerve injection of the PhRodo dye.

Fixed spinal cord tissue analysis by immunofluorescence histology

Double transgenic *Thy-1*$^{+/YFP}$ × *Cx3cr1*$^{+/GFP}$ or triple transgenic *Thy-1*$^{+/YFP}$ × *Cx3cr1*$^{+/GFP}$ × *Ccr2*$^{+/RFP}$ and *Thy-1*$^{+/YFP}$ × *Cx3cr1*$^{+/GFP}$ × *Ccr2*$^{RFP/RFP}$ mice were perfused with PBS followed by 4% PFA in PBS. Efficient perfusion was verified by blanching of the tissues. The tissue was then post-fixed in 4% PFA in PBS at 4 °C, embedded in OCT compound and cut to 20 μm thick slices. Endogenous RFP, GFP and YFP were used for imaging, and tissue was not counterstained with anti-fluorescent protein antibodies. Slides were mounted in Vectashield anti-fade solution (Vectorlabs) and imaged with a Leica SP5 confocal microscope (Leica).

Image processing and statistical analysis

Image processing was completed using Imaris (Bitplane) to identify axonal processes and track movement of cells. Mosaic images were compiled using XuvStitch (www.xuvtools.org/). Cellular infiltration and PhRodo inclusions were quantified via Imaris using the spots function (Bitplane) to automatically identify cells based on quality (greater than 1.2) and size of spots (greater than 6.7 μm in diameter). These numbers were the optimum suggested values from Imaris. Axonal dieback was quantified in 2D projections of mosaic images in ImageJ by measuring from the leading edge of the proximal stump of injured axons to the center of the lesion as identified by a line drawn between the center of the two insertion sites for the two forceps tines. "Destructive" events at the point of macrophage contact with the axon were identified when the width of the axon measured at the initial time of either cell contact or the initial point in our imaging session decreased or increased in width by more than 50% over the imaging session. Points of contact were identified by eye and measured only after cell contact was observed. Data analysis was performed blinded when possible, although data collection was not performed blinded for practical reasons. Movies were compiled using AfterEffects (Adobe). Statistical analysis was completed for the differences between final axonal positions, number of infiltrating cells, number of PhRodo inclusions seen within *Cx3cr1*$^{+/GFP}$ cells and migration speeds of monocytes and macrophages. In all cases, all tissue or images from a single animal was considered an N of 1. For example, if 3 sections from the same animal were used, this was considered an N of 1. All error bars are standard error of the mean. Paired Student's T-tests were used for all analyses in Excel (Microsoft). These tests are either single or double tailed as noted and assumed two samples of unequal variance.

Results

The influx of microglia and monocytes into the spinal cord lesion is closely correlated with axonal dieback

First, we sought to examine the DCC lesion using intravital 2-photon laser scanning microscopy. For these experiments, DCC was used since this injury has minimal functional impact on the animal and still enables us to visualize and measure axonal retraction and immune cell infiltration. This model consisted of a laminectomy followed by a 1 mm × 1 mm DCC injury to the dorsal columns at the T10 level (Fig. 1a). The injury severs ascending sensory axons while leaving larger blood vessels intact and minimizing fibroblast invasion (Fig. 1b). To visualize axons, monocytes and microglia at the site of injury *in vivo* without staining procedures, we bred *Thy-1*$^{+/YFP}$ *H* mice (Feng et al., 2000) and *Cx3cr1*$^{+/GFP}$ mice. To image these animals for all following experiments, we re-opened the spinal column at the site of injury. Re-opening surgeries up to 8 days after injury to gain access for imaging proved to be more reliable and introduced less inflammatory cell infiltration at the surgical site than chronic window implantation (data not shown).

This injury model reliably produced an easily quantifiable front of axons that die away from the center of the crush (Fig. 1c), replicated axonal dieback and inflammatory cell infiltration (Busch et al., 2009), and produced the same end ball morphology as shown by Ramon y Cajal (Cajal, 1907) (Fig. 1d). Axonal dieback was measured from the leading edge of the proximal stump of the damaged axon to the center of the crush site. The center of the site was identified as the line created between the center of the two tines of the forcep insertion points. The average difference in axonal position between 1 h after injury and 5 days after injury was 231.51 μm (Fig. 1e), concurrent with an infiltration of *Cx3cr1*$^{+/GFP}$ cells. *Cx3cr1*$^{+/GFP}$ cells increased in number at the edges and centers of lesions and were in close proximity to the ends of severed axons (Figs. 1c, f), roughly doubling in the first two days, increasing by 6 fold at day 5 and 9 fold at day 8. Results were not gender dependent as male and female mice were used. Next, we verified that

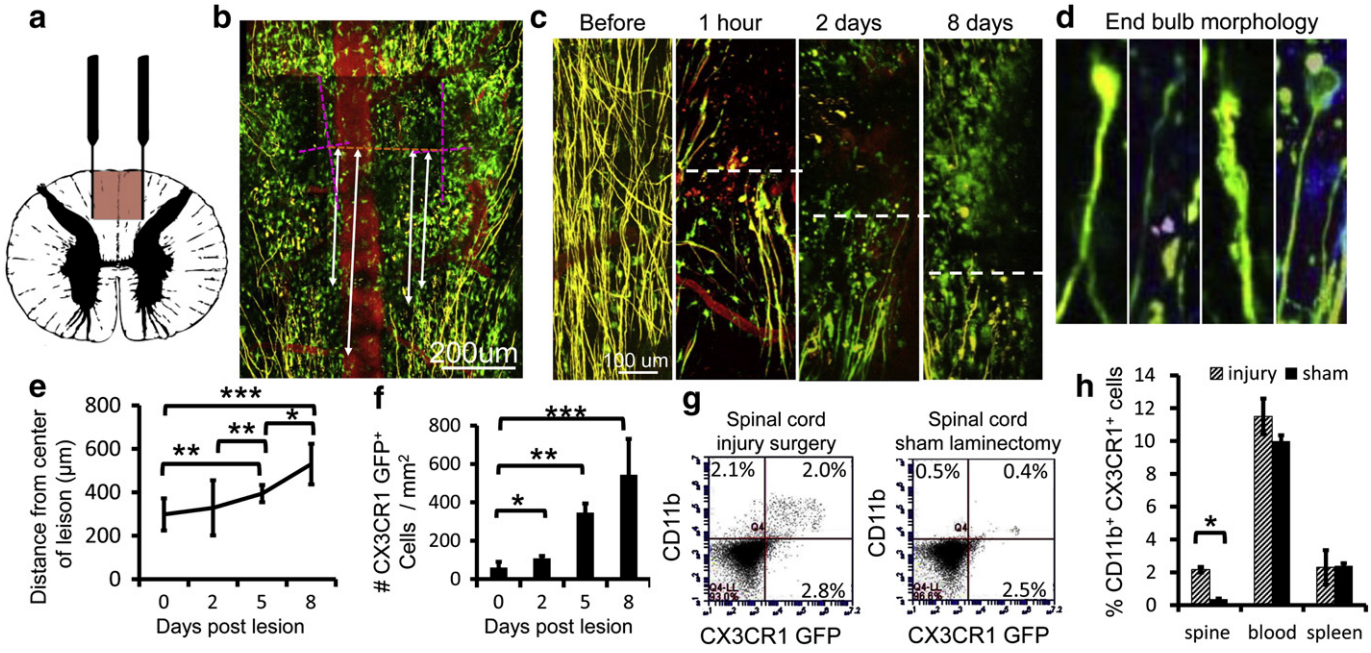

Fig. 1. Axons die back from the site of injury and macrophages infiltrate into a traumatic lesion of the dorsal columns in double transgenic Thy-1 and CX3CR1 GFP/+ mice. a) Diagram of the DCC injury. The red portion of the cord is damaged by a pinching motion of forceps. b) The DCC lesion was easily measured in double transgenic *Cx3cr1*$^{+/GFP}$ (green) × *Thy-1*$^{+/YFP}$ (yellow) animals with blood vessels labeled by intravenous TRITC-dextran vessel dye injection (red). The lesion is located by the insertion points of the two forceps tines (dotted pink lines). A line is then drawn between the centers of each insertion site to locate the center of the lesion (dotted orange line). Axon position is measured as the distance between axon tips and the orange line (white lines). Scale bar = 200 µm. c) Imaging of the DCC lesion in four separate animals before injury and during the first 8 days post injury reveals intact axons (yellow) in the dorsal column before injury and axonal retraction bulbs at progressively longer distances from the center of the lesion over time. After injury, the axonal position at the edge of the injury site is marked with a white dotted line. As time after injury increases, numbers of *Cx3cr1*$^{+/GFP}$ cells (green) within both the lesion border and the center of the lesion increase. Scale bar = 100 µm. d) Higher magnification of the end bulbs after injury, matching closely to those shown by Cajal (Cajal, 1907). e) Measurement of axon distances from center of DCC lesion. Axons die back an average of 336 µm over the first 8 days after injury. N = 3 at 0 and 2 days, N = 4 at 5 and 8 days. *P < 0.05, **P < 0.01, ***P < 0.001. f) Quantification of *Cx3cr1*$^{+/GFP}$ cell infiltration into center of DC lesion as in C. The number of CX3CR1$^{+/GFP}$ macrophages and microglia increases steadily over the first 8 days. N = 3 at 0 and 2 days, N = 4 at 5 and 8 days *P = <0.05 **P < 0.0001, ***P < 0.0002 g) Example of flow cytometry analysis of dissociated spinal cord 5 days after injury showing increased number of double positive, CD11b^{+} × *Cx3cr1*$^{+/GFP}$ cells found in the injured spinal cord, but not in an animal with a sham laminectomy. h) Flow cytometry analyses from blood, spleen and dissociated spine of *Cx3cr1*$^{+/GFP}$ mice 5 days after DCC injury compared to animals receiving a laminectomy but no injury. For both g and h, sample was gated to include all live cells in the sample of dissociated spinal cord. No additional purification steps were taken. Double positive *Cx3cr1*$^{+/GFP}$ / CD11b^{+} macrophage numbers remain the same in the blood and spleen but increased significantly in the spine 5 days after injury. Each condition was run in triplicate. * P < 0.05. All error bars are the standard error of the mean. P values are derived using a two-tailed t-test for two samples of unequal variance.

our time-lapse imaging procedures were not damaging to the tissue. We did not observe any adverse effects, *Cx3cr1*$^{+/GFP}$ macrophage infiltration or changes in *Cx3cr1*$^{+/GFP}$ cell morphology due to the imaging process over several hours. Both axons and the ramified morphology of microglia remained intact with no bubbling or increase in fluorescence as typically seen with thermal damage (Supplemental movie 1). Immediately after injury, time-lapse imaging revealed that *Cx3cr1*$^{+/GFP}$ cells began to extravasate from blood vessels and enter the lesion in the first hour after injury (data not shown).

CX3CR1 and CD11b double positive cells increase in number in spinal cord tissue after injury

To further verify the identity of *Cx3cr1*$^{+/GFP}$ cells within the lesion, we performed flow cytometric analysis of dissociated cells isolated from an area 1 mm rostral and 1 mm caudal to the lesion of injured and sham surgery spinal cords 5 days after injury. We verified the identity of the *Cx3cr1*$^{+/GFP}$ cells by staining for *CD11b/MAC1*, a marker for microglia, monocytes, macrophages and granulocytes in the CNS (Babcock et al., 2003) (Fig. 1g). In the spinal cord, there was a 6-fold increase in the number of double positive CD11b and GFP cells after injury (Fig. 1h). Cell numbers were not statistically different in the blood of DCC injured mice and sham animals (Fig. 1h).

Axonal dieback occurs by axotomy in the presence of Cx3cr1$^{+/GFP}$ *phagocytic cells*

We next investigated whether we could directly visualize the cellular process by which axons die back away from the lesion site and whether they lose parts of their retraction bulbs or retract into themselves during secondary dieback as they do *in vitro*. Again, we used double transgenic *Thy-1*$^{+/YFP}$ H × *Cx3cr1*$^{+/GFP}$ animals to identify axons, macrophages, and microglia, and imaged mice 2, 5 and 8 days after injury, during the period of secondary dieback. We observed large numbers of cell contacts between *Thy-1*$^{+/YFP}$ axons and *Cx3cr1*$^{+/GFP}$ cells. Surprisingly, some axon-macrophage contacts resulted in significant axonal morphologic changes and destruction during the 60 min following their initial interaction. An example is shown in Fig. 2a and Supplementary movie 2. We defined a destructive contact as one that causes a greater than 50% change in the width of the axon at the point of contact. We also observed destructive axonal contacts at 22 days after injury (Fig. 2b), indicating an ongoing process over a prolonged time period. There were averages of 3.14 ± 1.04, 3.28 ± 0.79 and 3.47 ± 1.41 *Cx3cr1*$^{+/GFP}$ cell contacts per 200 µm of axon per hour on days 2, 5 and 8 after injury, respectively (Fig. 2c). In total, we observed 305 individual contacts, of which 11 were destructive during one to two hour imaging sessions. Six of the destructive interactions resulted in axonal thinning and five resulted in a complete severing of the axon during the imaging session. These observations indicate that secondary dieback *in vivo* takes place by axotomy via contact with a *Cx3cr1*$^{+/GFP}$ cell. While there were many remnants of axons scattered about, the small percentage of observed contacts that ended in destruction of axons may be explained by the relatively short periods of observation that were possible in these animals. Many of the contacts we saw during the imaging period may have potentially resulted in a destructive interaction at later time points. Also, we have not observed any destructive events in axons without contact by a CX3CR1 positive cell, supporting the hypothesis that these two events are related. In support of an axonal

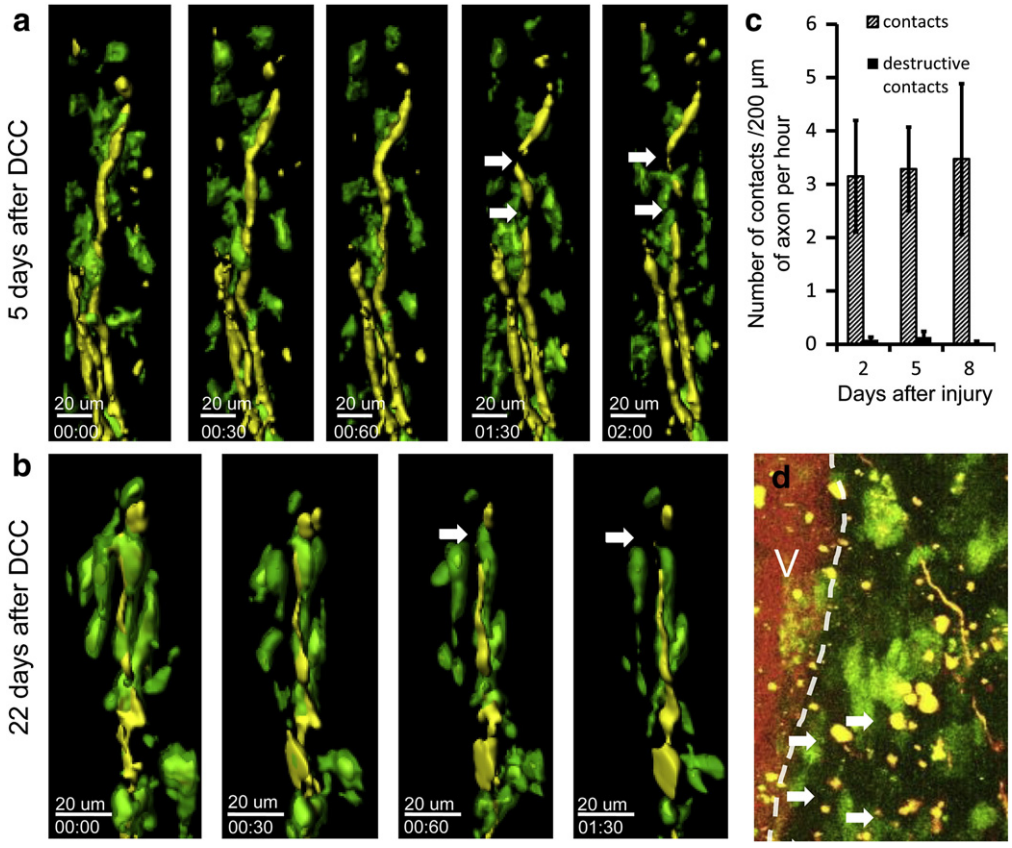

Fig. 2. *Cx3cr1*$^{+/GFP}$ cells contact axons in the dorsal column after initial DCC injury at sites of axonal thinning and breaking. Examples of axons (yellow) interacting with *Cx3cr1*$^{+/GFP}$ cells (green) at different times following DCC injury. Yellow axons are ascending dorsal column axons approaching the lesion. The lesion center is above the area shown. a) Example of interaction 5 days after DCC injury. Thinning and blebbing of the axon are marked by white arrows. Time stamp = h:min, total time 2 h. Scale bar = 20 µm. b) Example of an axonal cleavage 22 days after DCC injury. Cellular material can be seen separating from the end of the dystrophic axon after contact by a *Cx3cr1*$^{+/GFP}$ cell (white arrow). This indicates that loss of axonal bits is a continuing process even at later time points after injury. Time stamp = h:min. Total time: 1 h and 30 min. Scale bar = 20 µm. c) Quantification of the rate of *Cx3cr1*$^{+/GFP}$ cell contact with axons. Contacts were registered when a green *Cx3cr1*$^{+/GFP}$ cell remained less than 100 µm from an axon for more than 2 min. A destructive contact was registered when the width of the axon changed by more than 50% at a location with *Cx3cr1*$^{+/GFP}$ cell contact. Once a contact between a *Cx3cr1*$^{+/GFP}$ cell was identified, the width of the axon at the time of contact was measured in Imaris and compared to the width of the axon at the end of the imaging session or point where the contact ended, whichever came first. Non-destructive contacts (hashed bars) occurred more frequently than destructive ones, and increased on day 8 after DCC injury. Destructive contacts (black bars) were present in small numbers at 2, 5 and 8 days after injury. We observed a total of 45 contacts and 2 destructive contacts in 1.3 h of imaging in 3 animals at 2 days after injury, a total of 162 contacts and 6 destructive contacts in 4.65 h of imaging in 5 animals at 5 days after injury and total of 98 contacts and 3 destructive contacts in 5.4 h of imaging in 4 animals at 8 days after injury. Error bars are the standard error of the mean. d) Image of the lesion near axonal retraction bulbs at 5 days after injury. Axons (yellow), *Cx3cr1*$^{+/GFP}$ cells (green) and the dorsal vein (V, labeled with TRITC-dextran, red) can be seen. Yellow bits of axon material (arrows) can be seen in the lesion along the path that axons would have retracted along. These yellow inclusions are commonly seen along the edges of the lesion near retracting axons and appear to be parts of axons left behind during the process of axonal retraction. Scale bar = 50 µm.

shredding mechanism, bits of Thy-1^{YFP} axons were seen along the path of axonal dieback and within the lesion. An example at 5 days after injury is shown (Fig. 2d).

Cx3cr1$^{+/GFP}$ *cells phagocytize parts of once intact axons*

Next, we investigated whether initially intact portions of the damaged axon can be eventually phagocytized by *Cx3cr1*$^{+/GFP}$ cells between days 6 and 8 after DCC injury, at the time when a large portion of dieback takes place. We employed the pH-sensitive PhRodo-dextran conjugated dye (Invitrogen), which becomes fluorescent only in a low pH environment such as that found within lysosomes to identify phagocytized axonal structures. Use of the pH-sensitive red dye allowed us to separate inclusions within the GFP positive cells that were derived from phagocytosis of once intact dystrophic axonal ends from phagocytosis of debris generated during the formation of the lesion or debris from the portion of the axon undergoing Wallerian degeneration or from accidental detection of fluorescence in the yellow channel from very bright GFP emission. PhRodo-dextran (10 kD MW) was injected into the sciatic nerve unilaterally on day 6 after DCC injury (Fig. 3a). Two days later we observed puncta of fluorescent PhRodo dye within *Cx3cr1*$^{+/GFP}$ cells located on the same side of the spinal cord as the sciatic nerve injection (Figs. 3b and c). The average number of puncta on the side of injection was 43 ± 2, compared to 17 ± 10 puncta on the contralateral side ($P < 0.05$). Contralateral puncta may be in cells that migrated across the midline. Red puncta found outside the parenchyma of the spinal cord were excluded. Puncta within the spinal cord outside of CX3CR1$^{+/GFP}$ cells were not observed. We also observed Thy-1^{+} inclusions within the cytoplasm of *Cx3cr1*$^{+/GFP}$ cells, indicating that phagocytic uptake of axonal remnants by *Cx3cr1*$^{+/GFP}$ cells is not solely restricted to those containing PhRodo-dextran (Figs. 3d, e).

Blood-derived monocytes comprise the majority of mobile Cx3cr1$^{+/GFP}$ *cells within the lesion*

Since microglia are resistant to irradiation, and numbers of *Cx3cr1*$^{+/GFP}$ cells that can enter the CNS after irradiation are proportionately small (Ajami et al., 2007), we used a bone marrow chimera animal approach designed to distinguish the involvement of spinal cord-resident microglia or bone marrow-derived cells to observe the differences between these two cell types *in vivo* (Fig. 4a). Two variations of irradiation chimera animals were used. In the first, the host animal expressed *Thy-*

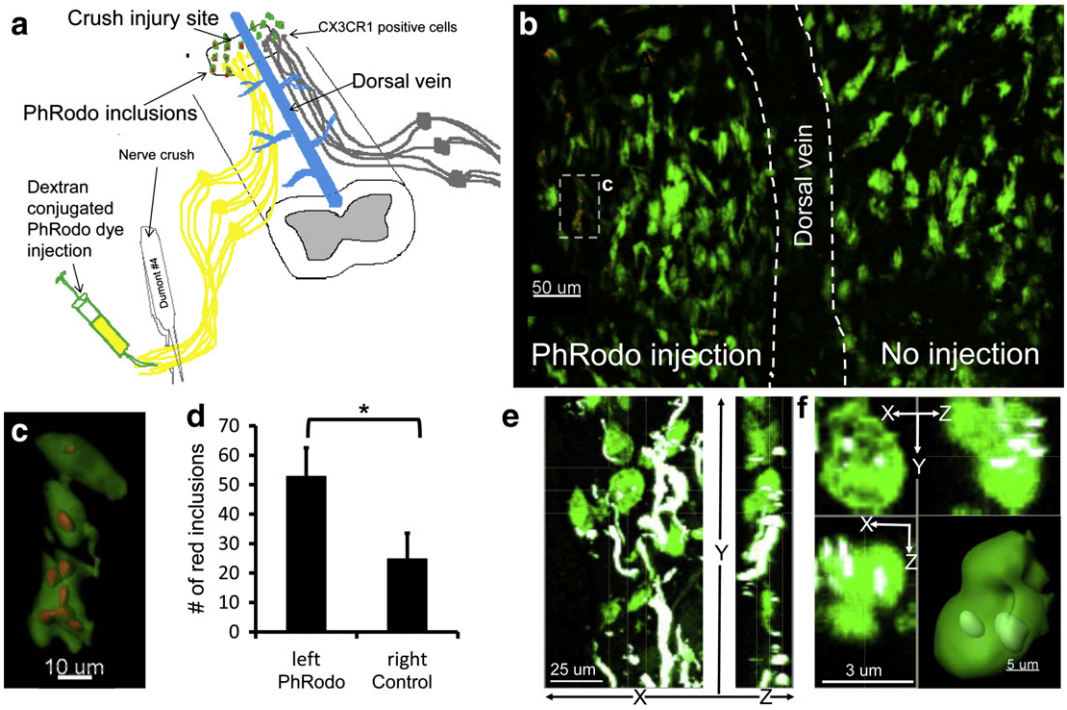

Fig. 3. CX3CR1^{+} cells phagocytize the ends of damaged dorsal column axons attached to the neuronal cell bodies in the dorsal root ganglia. a) Experimental scheme is depicted. PH-sensitive PhRodo-conjugated dextran (10,000 MW) was injected into the sciatic nerve unilaterally on day 6 following DCC injury. The dye was then taken up in the crushed sciatic nerve neurons and carried rostrally inside the neuron through the dorsal column to the site of DCC injury (yellow). The dye fluoresces red after phagocytosis and inclusion in a low pH lysosome. This allows us to distinguish axonal debris take up by macrophages that is removed from the ends of axons between days 6 and 8 from debris from the initial injury or from distal axons undergoing Wallerian degeneration. b) The PhRodo dye was seen inside *Cx3cr1*$^{+/GFP}$ phagocytic cells located within DCC lesion ipsilaterally to the sciatic injection. The average number of puncta on the side of injection was 43 ± 2, compared to 17 ± 10 puncta on the contralateral spine. c) Reconstruction of a *Cx3cr1*$^{+/GFP}$ cell seen in Fig. 3B with PhRodo dye inclusions, showing that these inclusions are within the green *Cx3cr1*$^{+/GFP}$ cells. d) Quantification of PhRodo inclusions in vesicles on the contralateral and ipsilateral side of the animal to dye injection. We observed a total of 53 inclusions on the ipsilateral side to injection and 25 inclusions on the contralateral side in a total of 3 *Cx3cr1*$^{+/GFP}$ mice. Error bars are standard error of the mean. *$P < 0.05$ using a two-tailed t-test assuming two samples of unequal variance. E) In the absence of PhRodo injection and sciatic nerve manipulation and any corresponding conditioning effects, *Thy-1*^{YFP} inclusions (white) can also be found within *Cx3cr1*$^{+/GFP}$ cells (green) near dystrophic axon ends (white) 5 days following DCC injury without manipulation of the sciatic nerve. CX3CR1^{+} cells were found along the ends of dystrophic axons. f) A single *Cx3cr1*$^{+/GFP}$ cell (green) with *Thy-1*^{YFP} inclusions (white) shown in E. X, Y and Z projections are shown, as well as a reconstruction of this cell showing the white inclusions within the *Cx3cr1*$^{+/GFP}$ cell.

1^{YFP} and the donor animal was heterozygous for *Cx3cr1*^{GFP}, allowing us to identify GFP^{+} macrophages. In the second, the host animal expressed both Thy-1^{YFP} and was heterozygous for *Cx3cr1*^{GFP} and the donor was a C57BL6 animal expressing no fluorescent proteins, allowing us to identify resident microglia. We also used a *Thy-1*$^{+/YFP}$ host with a double transgenic *Cx3cr1*$^{+/GFP}$ and *Ccr2*$^{+/RFP}$ donor to identify two lineages of blood-derived monocytes/ macrophages (Geissmann et al., 2003). We also checked for chimera efficiency at replacing monocytes in the blood of transplanted mice, confirming an average efficiency of replacement of 96% of the host *Cx3cr1*$^{+/GFP}$ blood cells with those from the donor (See Materials and methods for details). Spinal cord injury was performed 8–12 weeks after bone marrow transplantation to allow the immune system time to fully reconstitute. Using this approach, we did not observe any differences in the extent of axonal dieback or in the morphology of microglia, monocytes or axons within the lesion (Figs. 4b, c). At 2 h, 2 days, 5 days and 8 days after injury, we observed a large increase in blood-derived *Cx3cr1*$^{+/GFP}$ cells with very little increase in the *Cx3cr1*$^{+/GFP}$ resident cell population (Figs. 4d and e). We found that resident microglia appeared larger and more complex than monocytes and had simple extended processes, whereas monocytes were round (Fig. 4d). In the first hours after injury, we saw an insignificant difference between resident and infiltrating cells from that in the uninjured animal. Blood-derived cells increased by 3 fold from day 0 to 2 and 7 fold from day 0 to 8. There was no significant difference in the amount of resident cells at any time point after initial injury (Fig. 4e). These findings are in concordance with previous studies in contusion models in rat bone marrow chimeras and other models (Mawhinney et al., 2012; Popovich and Hickey, 2001; Popovich et al., 2003). Although irradiation of the spinal cord may attenuate proliferation of resident cells, these data revealed that the major increase in cellularity in the spinal lesion was attributed to infiltrating *Cx3cr1*$^{+/GFP}$ cells.

Monocyte-derived macrophages, not resident microglia, are responsible for secondary axotomy

Next, we looked to see if any behavioral properties varied between resident and infiltrating *Cx3cr1*$^{+/GFP}$ cells. Migratory capabilities of either monocytes or macrophages within traumatic spinal cord lesions have not been described previously. Using the same chimeric animals described in Fig. 4A, we observed differences in the speed and displacement of migration between blood-derived monocytes and resident microglia. The main population of *Cx3cr1*$^{+/GFP}$ cells within the lesion was composed initially of resident microglia that showed morphological activation. Within the first hour following injury, a small number of blood-derived *Cx3cr1*$^{+/GFP}$ cells began to extravasate from the blood vessels into the lesion, while resident microglia exhibited very little movement, as shown by tracks (Figs. 5a–c, Supplementary movie 3). A higher magnification of the movements of two blood-derived cells is shown in Fig. 5B. From the dynamic images, we measured speed and displacement. In the first hour and 8 days after injury the average speed of cord-resident microglia was 0.030 ± 0.0014 μm/s and 0.037 ± 0.0017, respectively, while these same measurements for blood-derived *Cx3cr1*$^{+/GFP}$ cells were 0.06 ± 0.0008 μm and 0.061 ± 0.0008 (Fig. 5d).

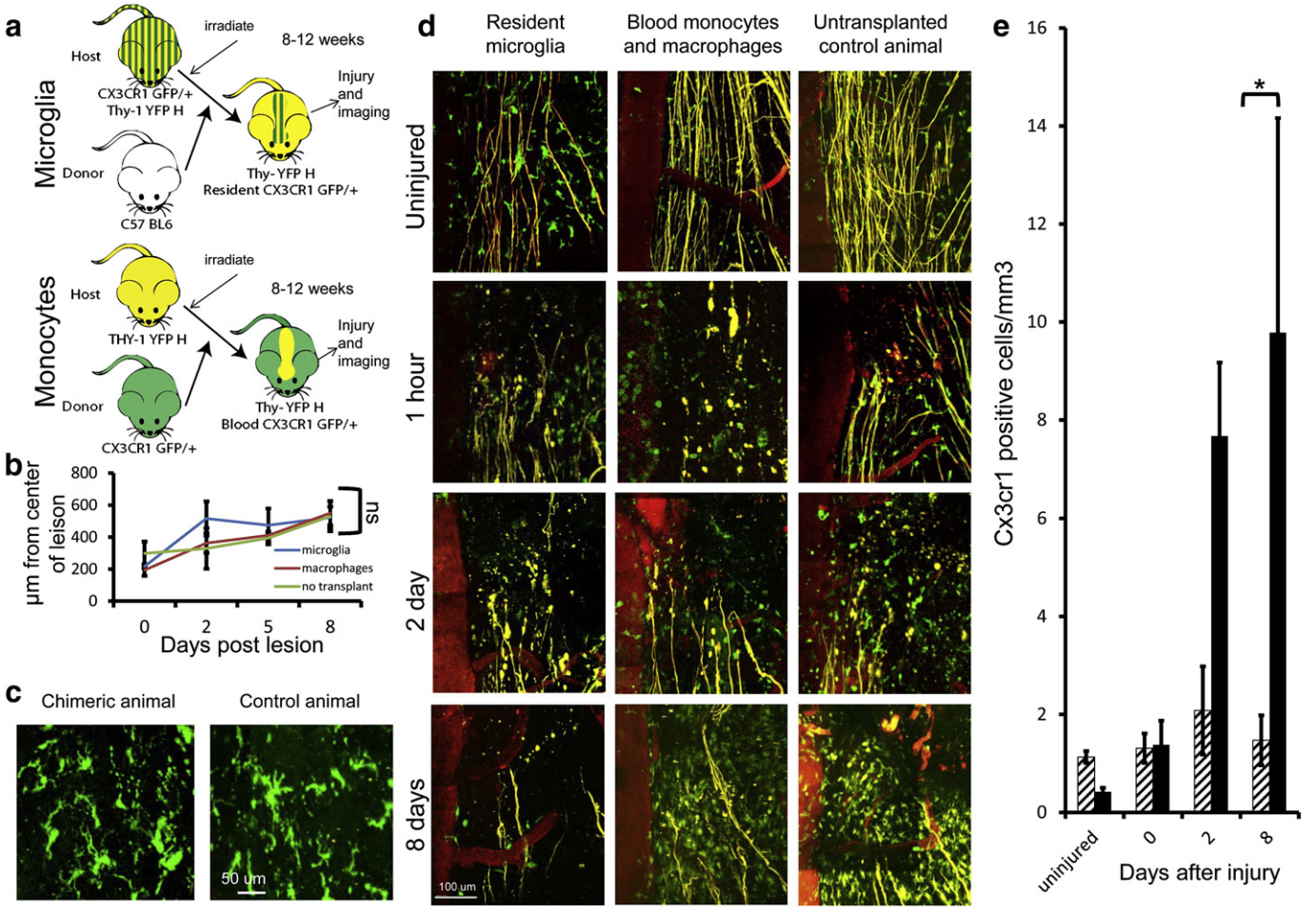

Fig. 4. The bulk of CX3CR1^{+} cells within DCC lesion are blood-derived. a) A schematic diagram of the bone marrow chimeric mice approach to allow for the distinction of blood-derived monocyte-lineage macrophages from resident microglia *Cx3cr1*$^{+/GFP}$ cells. Recipient mice were irradiated, reconstituted with donor-derived bone marrow cells and then allowed to rest for 8–12 weeks before imaging. *Cx3cr1*$^{+/GFP}$ × *Thy-1* $^{YFP/+}$animals received wild type B6 bone marrow, and *Thy-1* $^{YFP/+}$ animals received CX3CR1^{+} bone marrow, allowing only microglia or only blood-derived cells to be CX3CR1$^{+\cdot}$ b) Quantification of post-DCC axonal dieback in chimeric animals 8–12 weeks after transplant revealed no significant rate difference. All conditions have Ns of between 2 and 7. The average N is 4. A total of 639 axons in 98 mice were imaged. c) Comparison of microglia in chimeric animals with a *Cx3cr1*$^{+/GFP}$ host and a B6 donor and *Cx3cr1*$^{+/GFP}$ animals shows similar morphology. Scale bar is 50 µm. Non-significance was determined using a two-tailed t-test assuming two sample of unequal variance. d) Images of the caudal aspect of the DCC lesion in *Thy-1*$^{YFP/+}$ chimeric animals with either labeled host or donor *Cx3cr1*$^{+/GFP}$ cells as compared to non-chimeric, un-irradiated double transgenic *Thy-1*^{YFP} × *Cx3cr1*$^{+/GFP}$ animals. The first column shows animals with *Cx3cr1*$^{+/GFP}$ hosts and B6 donors, showing resident microglia. Small numbers of *Cx3cr1*$^{+/GFP}$ positive cells are present in the lesion at all time points. The center column shows animals with *Cx3cr1*$^{+/GFP}$ donor cells, showing blood-derived *Cx3cr1*$^{+/GFP}$ monocytes and macrophages that rapidly increase in number with increasing time after injury. The right column shows non-chimeric double transgenic *Thy-1*^{YFP} × *Cx3cr1*$^{+/GFP}$ animals. e) Quantification of cell numbers in the center of the lesion in E revealed consistently few microglia (hashed bars), but a dramatic increase in monocyte-derived cell number (black bars) over 8 days. Microglia numbers remain stable over time, and infiltrating macrophages increase dramatically over time. All conditions have Ns of between 2 and 7. The average N is 4. Number of microglia and macrophages at the same time point are statistically different at days 2 and 8 after injury. *P < 0.02 using a one tailed *T*-test assuming two samples of unequal variance.

In the first hour and 8 days after injury the average displacement of cord-resident microglia was 4.47 ± 0.22 µm and 5.51 ± 0.40, respectively, while these same measurements for blood-derived *Cx3cr1*$^{+/GFP}$ cells were 15.4 ± 0.32 µm and 14.35 ± 0.40 (Fig. 5e). In the images shown in a and c, differences in directionality of blood-derived cell movement can be observed through the time-coding of cell position shown by the changing color of the tracks. Using this coding, the earliest times in imaging are identified as blue and the latest time points are identified as white. In the first hour after injury, cells were primarily localized within the vessel lumen at the beginning of the imaging period and were seen to migrate from the blood vessel and into the lesion by the end of the 60-minute imaging period (Fig. 5a). No directional migration of cells towards either the proximal or distal portion of the lesion was noticed. This migration from the dorsal vein in the spinal cord was only seen immediately after injury. At later time points, there was a decrease in cell migration within the perivascular region and an increase in migration within the center of the lesion. No directionality or focus of movement of cells within the center of the lesion at these later time points was noted, or expected due to the amount of tissue damage seen throughout the lesion (Fig. 5c). Directionality of movement was also difficult to assess due to movement of cells into and out of the field of view and large populations of stationary or near stationary CX3CR1$^{+/GFP}$ cells.

Next, we observed the cell contacts between these blood-derived and resident *Cx3cr1*$^{+/GFP}$ cells within the lesion in the chimeric animals to see if a subset of these was responsible for destructive contacts. In one case, we observed a quickly moving *Cx3cr1*$^{+/GFP}$ cell at the lesion edge contacting an axon in two places, in each case with a destructive effect (Fig. 6a and Supplementary movie 4). In another example, the axon was completely severed (Fig. 6b). We did not observe any destructive changes where microglia contacted axons (Figs. 6c, e). We observed a total of 232 contacts and 22 destructive contacts in 10 *Cx3cr1*$^{+/GFP}$ → WT chimeric mice (Figs. 6a, b and d). We observed a total of 52 contacts and no destructive contacts in 11 WT → *Cx3cr1*$^{+/GFP}$ chimeric mice (Figs. 6 c and e). These data indicate that destructive contacts largely, but perhaps not entirely, occur between blood-derived cells and axons.

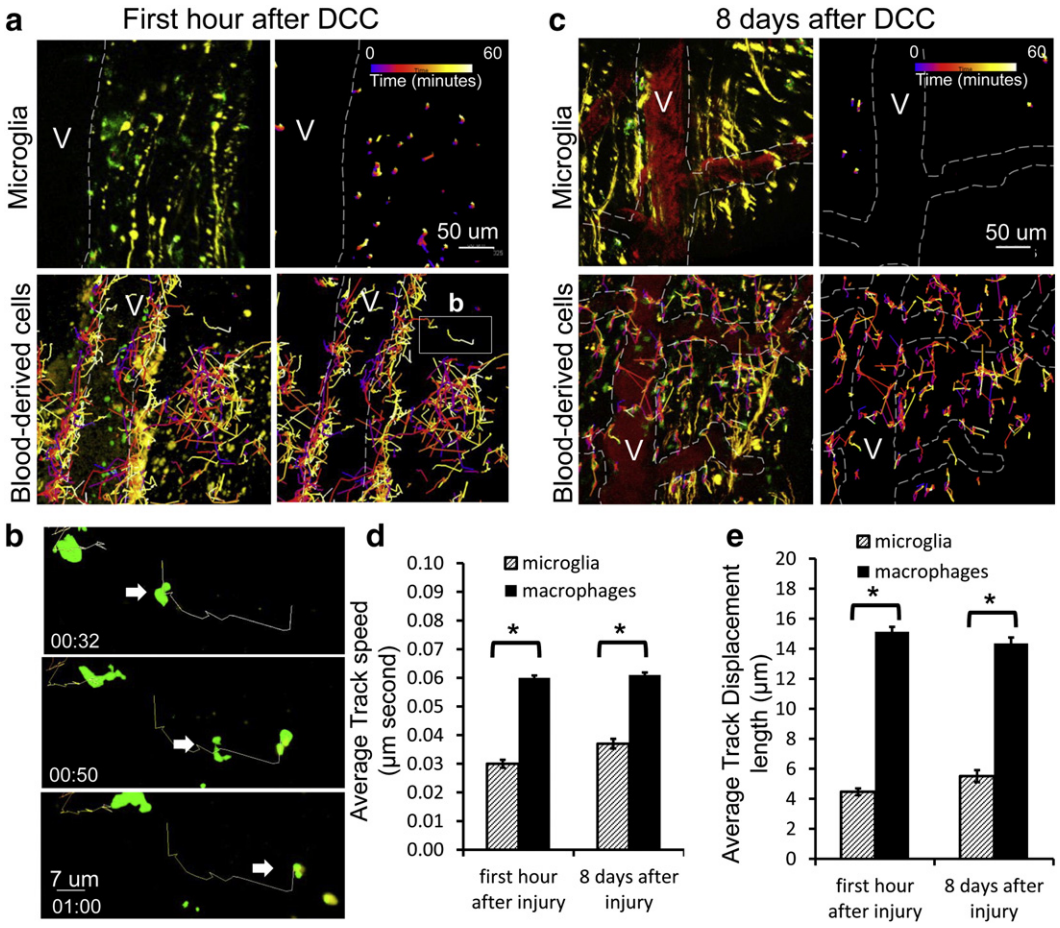

Fig. 5. Blood-derived CX3CR1^{+} cells have greater average speed and displacement than resident microglia. a) Immediately after DCC lesion, *Cx3cr1*$^{+/GFP}$ microglia move only very short distances, while blood-derived cells traversed over great distances within the center of the lesion. Cell tracks are shown as color-coded time stamps (blue: time = 0 min; yellow: time = 60 min; gradient shown in the figure). Both tracks and fluorescence are shown in images on the left, and only tracks in images on the right. Scale bar = 50um. Total time for tracking is 1 h. b) High-magnification sequential images of a one macrophage's track and movement in a. Scale bar = 7 um. Time stamp: h:min. Total time shown is 28 min. c) 8 days after DCC, only a few stationary microglial cells were found within the lesion 8 days following DCC injury. In comparison, blood-derived cells traveled over greater distances near the lesion. Both tracks and fluorescence are shown in images on the left, and only tracks in images on the right. Time stamp is the same as in a. Scale bar = 50um. d) In the first hour after injury and at 8 days after injury, monocytes and macrophages have a higher average speed than microglia. Each track was assessed for average speed. Tracking results were obtained from 228 microglia and 1601 monocytes/macrophages cells in three animals for each condition *P < 0.00001. e) In the first hour after injury and at 8 days after injury, monocytes and macrophages have a larger average displacement than microglia. Tracking is from 228 microglia and 1601 monocytes/macrophages cells in three animals for each condition *P < 0.00001.

Blood-derived CX3CR1$^{GFP/+}$ *cells are very rarely also CCR2*$^{RFP/+}$ *and axonal position after injury is not dependent on CCR2 expression*

To further clarify the identity of infiltrating CX3CR1 phagocytic cells, we took advantage of differential expression of CCR2 and CX3CR1 that can identify different subsets of circulating macrophages (Mahad et al., 2006; Saederup et al., 2010). We did not observe any destructive events in axons outside of CX3CR1 positive cell contact, so we looked in fixed tissue sections to see if these CX3CR1 positive blood-derived cells were also CCR2 positive. To this end, we generated chimeric animals with a *Thy-1*$^{+/YFP}$ host and *Ccr2*$^{+/RFP}$ × *Cx3cr1*$^{+/GFP}$ marrow donor. In fixed sections from the transplanted animal in which we were able to observe CCR2 RFP using confocal imaging, CX3CR1 and CCR2 fluorescence was restricted to only blood-derived monocytes and macrophages but not microglia. Both *Ccr2*$^{+/RFP}$ cells and *Cx3cr1*$^{+/GFP}$ cells were blood derived and capable of infiltrating into the lesion following spinal trauma, while virtually no *Ccr2*$^{+/RFP}$ cells were found at sites away from the lesion. *Ccr2*$^{+/RFP}$ cells were round in appearance resembling monocyte morphology while *Cx3cr1*$^{+/GFP}$ cells were larger with granular cytoplasm consistent with tissue phagocytes in both the normal and transplanted animals (Fig. 7a). The infiltrating cells comprise three populations in the chimeric animals. CCR2 single positive cells comprised the largest population, followed by CX3CR1 single positive cells. There was also a very small population of double positive cells within the lesion (Fig. 7b), possibly comprised of CCR2 cells that are in the process of down regulating CCR2 and upregulating CX3CR1 as macrophages mature. Since we observed destructive contacts with *Cx3cr1*$^{+/GFP}$ positive cells (Figs. 2, 6) and the double-labeled infiltrating cells were a small minority (Fig. 7b), we speculate that destructive contacts were initiated by the subgroups of infiltrating cells that are *Cx3cr1*$^{+/GFP}$ positive, and not those that are *Ccr2*$^{+/RFP}$ single positive. This was not directly tested due to the dimness of CCR2$^{RFP/+}$ cells in our live imaging set-up. Next, to verify that these CCR2 positive cells are unlikely to be involved in axonal dieback, we looked at the axonal position 5 days after DCC in triple transgenic Thy-1^{YFP}, CX3CR1$^{GFP/+}$ and either CCR2$^{RFP/+}$ or CCR2$^{RFP/RFP}$ animals (Figs. 7c, d). In this case, we did not see any difference in axonal position when measured from the leading edge of the proximal stump of the axon leading up to the injury (Fig. 7e), indicating that CCR2 is not directly necessary for axonal dieback.

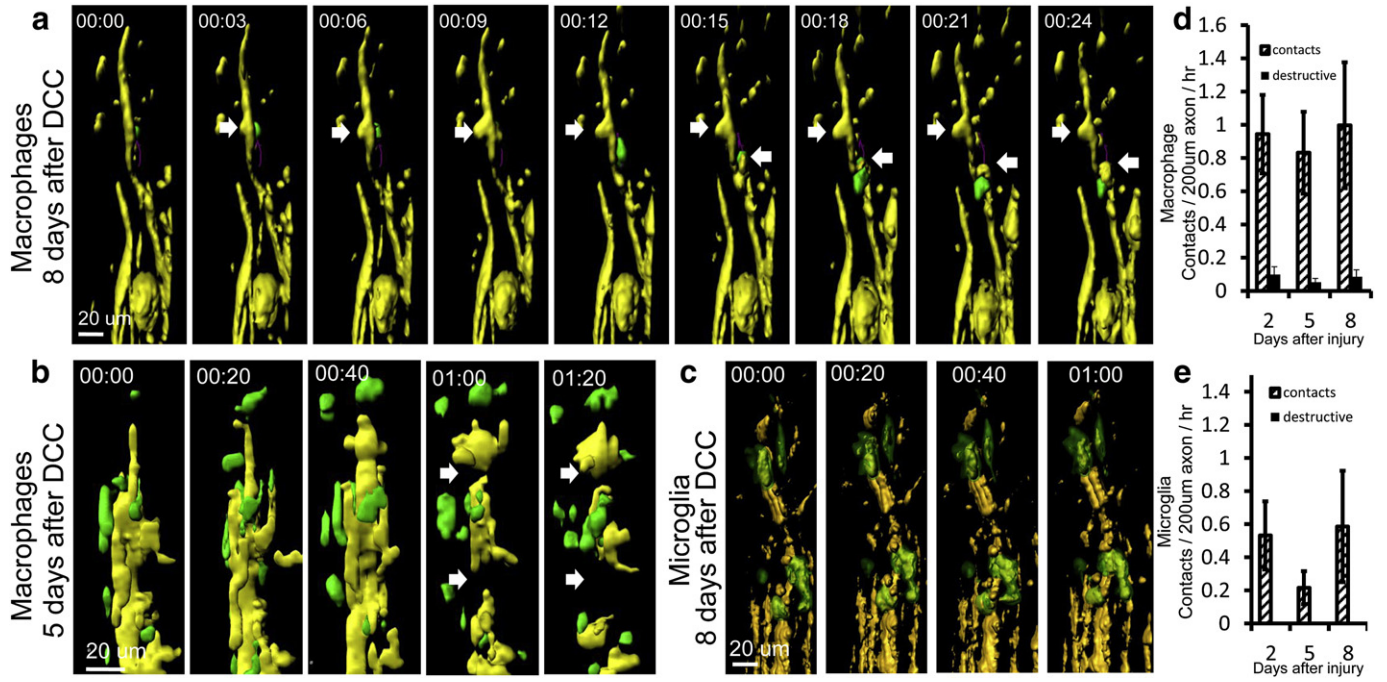

Fig. 6. Axonal destruction occurs in response to contact only with *Cx3cr1*$^{+/GFP}$ blood-derived cells and not *Cx3cr1*$^{+/GFP}$ microglia. a) Example of contact between a *Thy-1*$^{CFP/+}$ axon (yellow) and a *Cx3cr1*$^{+/GFP}$ blood-derived cell (green) resulting in axonal "blebbing" (white arrows) on day 5 after DCC injury. Blebbing occurred in two locations of the axon (yellow). b) Another example of a contact between a *Thy-1*$^{YFP/+}$ axon (yellow) and a *Cx3cr1*$^{+/GFP}$ blood-derived cell (green) resulting in axonal breakage (white arrows) on day 8 after DCC injury. c) Example of the interactions between microglia (green) and an axon (yellow) on day 8 after DCC injury. No change in axonal size or integrity was observed during an hour-long imaging session. Colors here are different than in A and B to allow easier identification of yellow axons. d) Quantification of contacts between axons and blood-derived macrophages, with steady numbers of contacts and destructive contacts between axons and monocytes/macrophages seen on days 2, 5 and 8. We observed a total of 232 contacts and 22 destructive contacts in 10 blood-derived *Cx3cr1*$^{+/GFP}$ mice. e) Quantification of contacts between axons and resident microglia, with contacts but no destructive contacts seen on days 2, 5 and 8. We observed a total of 52 contacts and no destructive contacts in 11 resident *Cx3cr1*$^{+/GFP}$ mice.

Discussion

Mechanism of secondary dieback by axonal membrane loss

We observed that axonal retraction during the secondary injury phase occurs via multiple axotomies along the distal portion of injured stalled axons which, in turn, results in the removal of the end of the axon, creating a new axonal end. In contrast to this, *in vitro* activated macrophages caused retraction of dystrophic axons over a long distance in a manner involving rapid dissolution of the axonal cytoskeleton, causing the distal axon to rapidly retract into itself (Horn et al., 2008). This difference in mechanism is not surprising, as neuron behavior *in vitro* occurred without the influence of extracellular matrix and surrounding support cells. Similar axotomy and loss of axonal membrane during dieback instead of axonal involution has been proposed to occur in the CNS parenchyma following several other models of injury where macrophages interact with injured axons. These include zymosan injection (Fitch and Silver, 2008) and traumatic brain injury (Greer et al., 2013). Furthermore, our real-time observations of blebbing and loss of membrane from axonal ends is consistent with the suggested pattern of axonal dieback in the cortex after an ischemic stroke, where axonal debris is found at the location where the uninjured axon was present before the axon retracted towards its cell body and away from the site of injury (Hawthorne et al., 2011). Axonal thinning has also been shown in models of EAE (Powers et al., 2012). Our observations provide further distinction between the initial phase of axonal retraction that is cell intrinsic and decreased in the Wallerian degeneration slow mouse (Kerschensteiner et al., 2005) and the secondary, inflammatory phase of retraction.

Removal of membrane from axonal ends may have increased significance in the context of sprouting and attempted regrowth of axons within the core of the lesion. Axonal ends in the lesion are not stationary (Busch et al., 2009) and attempt to sprout in the first few days to weeks after injury (Kerschensteiner et al., 2005) largely in association with NG2 glia whose surface is preferred by dystrophic axons and upon which the dystrophic axon tips eventually stabilize and form synaptic-like connections (Busch et al., 2010; Filous et al., 2013). It is possible that activated macrophages, in addition to causing axonal dieback at early stages, may also be involved in curtailing the ability of axons to sprout. It is also possible that macrophages move from neuron to neuron over a longer time period, removing membrane continually in a fashion similar to the process of synaptic pruning that occurs during development (Schafer et al., 2012, 2013).

Since infiltrating cells appear to be damaging, we looked at CCR2 and CX3CR1 markers in fixed tissue to differentiate monocytes expressing these two chemokine receptors (Saederup et al., 2010). The CCR2^{hi}/CX3CR1^{lo} population of monocytes differentiates into macrophages or dendritic cells, while the CCR2^{lo}/CX3CR1^{hi} population may aid in wound healing and other functions (Geissmann et al., 2003). Although speculative, it appears that the *CCR2*$^{+/RFP}$ cell population is less likely to be involved in dieback as we have not seen axonal destruction events that are not associated with contact by a *Cx3Cr1*$^{+/GFP}$ cell. Therefore, since few *Cx3Cr1*$^{+/GFP}$ cells are also *CCR2*$^{+/RFP}$ positive, we can infer that these cells are less likely to be involved in destructive events. This supports the idea that there are subtypes of macrophages that may be more or less harmful during trauma, and increasing the population that does not cause destruction may be therapeutic (Kigerl et al., 2009). The distinction between these subtypes of macrophages and microglia is especially interesting, since it supports the idea that microglia are involved primarily in maintaining CNS homeostasis, and continue to perform such functions even after a traumatic injury (Davalos et al., 2005).

Separating the two main *Cx3cr1*$^{+/GFP}$ positive monocyte and microglial cell lineages in the spinal cord presents a technical challenge. Most models to-date involve manipulation of the animals, which could cause potential permanent changes in the CNS cellular architecture. These manipulations included an *in utero* transplantation chimera

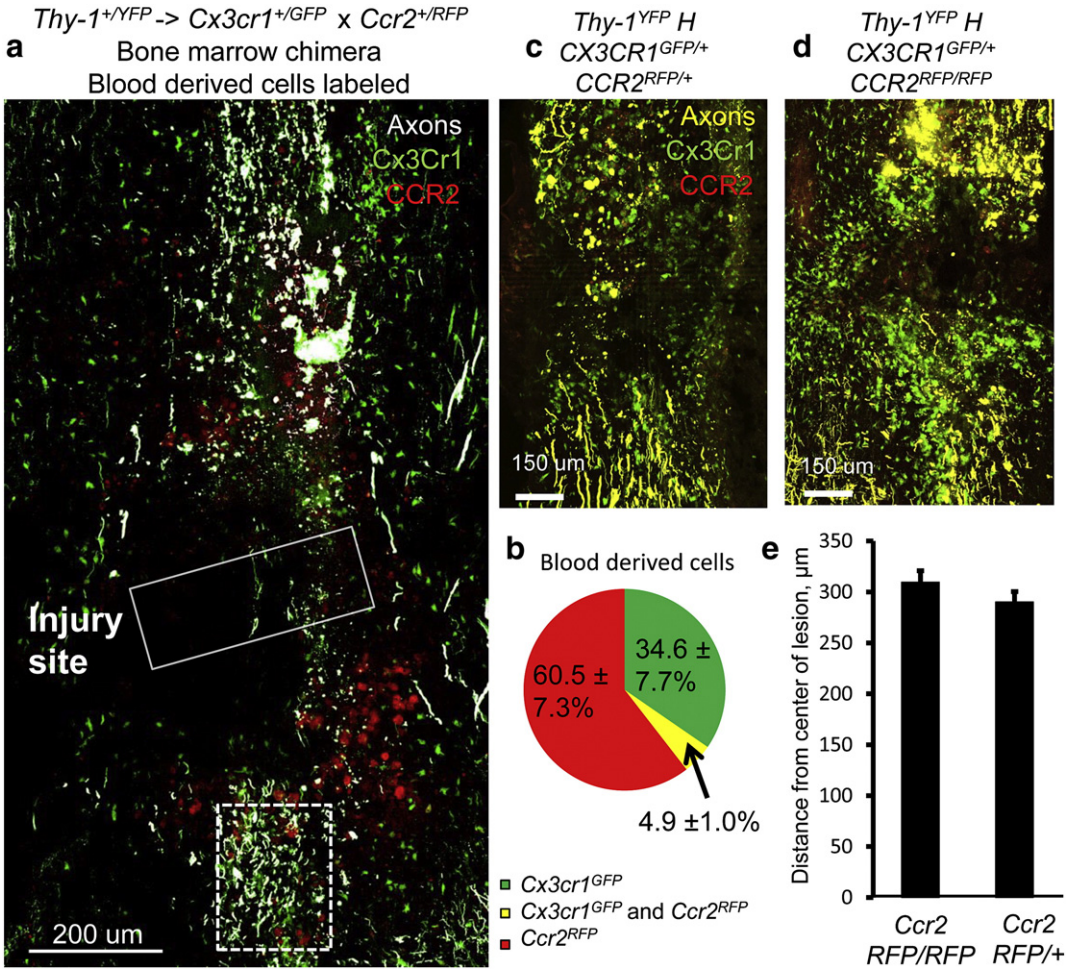

Fig. 7. Very few macrophages are both Cx3cr1 $^{+/GFP}$ and *Ccr2*$^{+/RFP}$ positive. Resident microglia are primarily Cx3cr1 $^{+/GFP}$, while blood-derived macrophages consist of populations of both Cx3cr1$^{+/GFP}$ positive macrophages and *Ccr2*$^{+/RFP}$ positive macrophages. Axonal position after dieback is not affected by CCR2 deficiency. Since all instances of axon thinning and breaking in *in vivo* imaging were in contact with a *Cx3cr1*$^{+/GFP}$ cell, we wanted to see if these cells are part of the same or different population than CCR2^{+} macrophages. a) Compiled immunofluorescence images of a DCC lesion (solid white box) 5 days after injury in fixed, sectioned tissue in a *Thy-1*$^{+/YFP}$ (white) × *Cx3cr1*$^{+/GFP}$ (green) × *Ccr2*$^{+/RFP}$ (red) triple-reporter mouse. A caudal region containing degenerating axons is marked with a dotted white box. Cx3cr1$^{+/GFP}$ and *Ccr2*$^{+/RFP}$ cells are found around the lesion. Scale bar is 200um. b) Quantification of *Cx3cr1*$^{+/GFP}$ (green) and *Ccr2*$^{+/RFP}$ (red) blood-derived cells found in the lesion in chimeric mice. Quantification is performed in three slices in each of three mice. c) A triple transgenic animal 5 days after DCC expressing *Thy-1*^{YFP}, *Cx3cr1*$^{+/GFP}$ and *Ccr2*$^{RFP/+}$. Scale bar = 100 µm. d) A triple transgenic animal 5 days after DCC expressing *Thy-1*^{YFP}, *Cx3cr1*$^{+/GFP}$ and *Ccr2*$^{RFP/RFP}$. Scale bar = 100 um. e) Quantification of axon position from the center of the lesion in these animals as described in the Materials and methods. N = 5 for each condition. P = 0.10 using a one tailed *t*-test assuming samples of unequal variance. There is no difference between *Ccr2*$^{RFP/+}$animals and *Ccr2*$^{RFP/RFP}$ animals, indicating that *Ccr2* is also not singly responsible for axonal position after injury. Since we only observed destructive events with *Cx3cr1*$^{+/GFP}$ cells in time-lapse imaging, and no difference in dieback is see in CCR2 deficient animals, we can infer that the *Ccr2*$^{+/RFP}$ cells, although present in the lesion, are unlikely to be responsible for these destructive events.

model (Nijagal et al., 2011), a head-shielding radiation model (Shechter et al., 2009), busulfan chimeras (Kierdorf et al., 2013a), parabiosis (Ajami et al., 2011), macrophage depletion by clodronate liposomes (Horn et al., 2008), and labeling of monocytes with CCR2^{RFP} (Ma et al., 2002; Saederup et al., 2010). None of these approaches, including ours, are without caveats. Many of them are technically challenging and may not have high enough efficiency to distinguish the two cell types. Irradiation has also been shown to reduce microglial activation for the first week in the retina (Bosco et al., 2012), which may persist. Busulfan is a chemotherapy drug that can be used to ablate host bone marrow in place of irradiation. Busulfan chimeras have reduced infiltration into the CNS and blood brain barrier effects than irradiation chimeras, although peripheral cell recruitment to the facial nerve after axotomy is drastically reduced (Kierdorf et al., 2013a), making the study of infiltrating cells more difficult. Clodronate liposomes subject the animal to inflammation associated with death of the cells (Van Rooijen and Sanders, 1994), preventing simple observation in an otherwise normal animal. In our hands we did not observe any irreparable differences between control animals and bone marrow chimeras in terms of the degree of axonal dieback or changes in cell morphology, suggesting that our techniques are as minimally invasive as possible.

Further investigating knockout of chemokine receptors

In *Ccr2*$^{RFP/RFP}$ animals, a decrease in macrophage infiltration into tissue has been observed in many models including corneal injury (Oshima et al., 2006), EAE (Gaupp et al., 2003), *toxoplasma gondii* infection (Dunay et al., 2008) and neuropathic pain (Abbadie et al., 2003). In cases where there is still some macrophage infiltration, there are also other chemokines that may be able to compensate for loss of CCR2 (Gaupp et al., 2003). Again, we observed an infiltration of *Cx3cr1*$^{+/GFP}$ and CCR2$^{+/RFP}$ cells into the lesion in CCR2 deficient animals, and no change in axonal position. In this case, it is likely that we do not see a change in axonal position simply because the CX3CR1^{hi} cells involved in axonal dieback are still able to migrate into the lesion independent of CCR2.

A second chemokine that will need to be investigated in the future is CX3CR1, which is involved in monocyte motility and is the only known

receptor for Fractalkine, a chemokine that is expressed on neurons and peripheral endothelial cells (Yona et al., 2013),. Varying degrees of differences in disease progression and severity have been documented between *Cx3cr1*$^{GFP/GFP}$ and *Cx3cr1*$^{+/GFP}$ animals in a variety of mouse models of disease and injury. These range from no difference in mouse models of facial axotomy (Jung et al., 2000), to larger changes in Alzheimer's disease (Bhaskar et al., 2010; Lee et al., 2010), spinal cord injury (Donnelly et al., 2011), multiple sclerosis (Huang et al., 2006), amyotrophic lateral sclerosis (ALS) and Parkinson's disease (Cardona et al., 2006). Although not investigated here, a comparison of axonal dieback between CX3CR1$^{GFP/GFP}$ and CX3CR1$^{+/+}$ animals will be instructive to the understanding of these cellular interactions. Future experiments in another model of dieback, such as in the rat, where greater retraction distances occur may be helpful (Horn et al., 2008). Perhaps inhibiting more than one chemokine receptor at the same time will add specificity to the well-established data suggesting that global macrophage depletion can inhibit secondary dieback.

Further investigating destructive cell types within the lesion

Even though we have identified *Cx3cr1*^{hi} macrophages as the cell population responsible for secondary axonal dieback, we have yet to define the molecular signals involved in this process or the significance of the *Cx3cr1*^{lo} and *Ccr2*^{hi} cells in the lesion. Furthermore, the activation state of the macrophage may also be important, as *Cx3cr1*$^{+/GFP}$ macrophages early on within the DCC lesion may be activated in a way that promotes phagocytosis and removal of damaged tissues and potential pathogens or later on in a way that promotes healing and scar tissue formation (Kigerl et al., 2009).

Many molecular signaling candidates involved in the macrophage–dystrophic axon interaction have been proposed, including receptors for phosphatidylserine (Titsworth et al., 2008) such as milk-fat globule epidermal growth factor-like factor 8 (MFG-E8) (Li et al., 2012). Signaling may also occur via changes in membrane permeability through perforin or calcium-mediated processes (Coleman, 2005). Blockade of proteases such as MMP9 has been used to prevent axonal retraction *in vitro*, arguing that dieback may require protease action between macrophages and dystrophic axons (Busch et al., 2009). Chemotaxis may also be an important contributor in recruiting relevant cells to the correct sites. Although we have determined that, in this model, CCR2 is not necessary for this secondary axonal dieback phenotype, other chemoattractants are likely involved. Further investigation into what these signaling pathways are in traumatic lesion is warranted, as well as the mechanism of interaction between the macrophage and axon. Separating these two subpopulations of cells and elucidating their roles in secondary damage will play a large role when approaching more specific interventions for treatment of spinal cord injury.

Supplementary data to this article can be found online at http://dx.doi.org/10.1016/j.expneurol.2014.01.013.

Acknowledgments

The following agencies provided critical funding support for this study: MSTP T32 GM007250 (T.A.E.), 5T32EB7509 (D.S.B.), NINDS R01 NS25713 (J.S.), NCI R01 CA154656 (A.Y.H.), Dana Foundation (A.Y.H.), St. Baldrick's Foundation (A.Y.H.), Alex's Lemonade Stand Foundation (A.Y.H.), Gabrielle's Angel Foundation (A.Y.H.) and Hyundai Hope-on-Wheels Research Program (A.Y.H.). The authors are grateful to Dr. Izzy Charo, M.D., Ph.D. for the use of the CCR2 RFP mice, Hongmei Hu for technical help with genotyping, Ross Anderson for mounting the spinal stabilizing unit and Dr. Richard Zigmond, Ph.D., Dr. Marcello Chieppa, Ph.D. and Marc DePaul for thorough review and thoughtful critiques of the manuscript.

References

Abbadie, C., Lindia, J.A., Cumiskey, A.M., Peterson, L.B., Mudgett, J.S., Bayne, E.K., DeMartino, J.A., MacIntyre, D.E., Forrest, M.J., 2003. Impaired neuropathic pain responses in mice lacking the chemokine receptor CCR2. Proc. Natl. Acad. Sci. U. S. A. 100, 7947–7952.

Ajami, B., Bennett, J.L., Krieger, C., Tetzlaff, W., Rossi, F.M., 2007. Local self-renewal can sustain CNS microglia maintenance and function throughout adult life. Nat. Neurosci. 10, 1538–1543.

Ajami, B., Bennett, J.L., Krieger, C., McNagny, K.M., Rossi, F.M., 2011. Infiltrating monocytes trigger EAE progression, but do not contribute to the resident microglia pool. Nat. Neurosci. 14, 1142–1149.

Babcock, A.A., Kuziel, W.A., Rivest, S., Owens, T., 2003. Chemokine expression by glial cells directs leukocytes to sites of axonal injury in the CNS. J. Neurosci. 23, 7922–7930.

Bhaskar, K., Konerth, M., Kokiko-Cochran, O.N., Cardona, A., Ransohoff, R.M., Lamb, B.T., 2010. Regulation of tau pathology by the microglial fractalkine receptor. Neuron 68, 19–31.

Bosco, A., Crish, S.D., Steele, M.R., Romero, C.O., Inman, D.M., Horner, P.J., Calkins, D.J., Vetter, M.L., 2012. Early reduction of microglia activation by irradiation in a model of chronic glaucoma. PLoS One 7, e43602.

Busch, S.A., Horn, K.P., Silver, D.J., Silver, J., 2009. Overcoming macrophage-mediated axonal dieback following CNS injury. J. Neurosci. 29, 9967–9976.

Busch, S.A., Horn, K.P., Cuascut, F.X., Hawthorne, A.L., Bai, L., Miller, R.H., Silver, J., 2010. Adult NG2+ cells are permissive to neurite outgrowth and stabilize sensory axons during macrophage-induced axonal dieback after spinal cord injury. J. Neurosci. 30, 255–265.

Cajal, S.R.Y., 1907. Structure et connexions des neurones. Nordiskt Medicinskt Arkiv 40(2). Nordiskt Medicinskt Arkiv 40, 1–28.

Cardona, A.E., Pioro, E.P., Sasse, M.E., Kostenko, V., Cardona, S.M., Dijkstra, I.M., Huang, D., Kidd, G., Dombrowski, S., Dutta, R., Lee, J.C., Cook, D.N., Jung, S., Lira, S.A., Littman, D.R., Ransohoff, R.M., 2006. Control of microglial neurotoxicity by the fractalkine receptor. Nat. Neurosci. 9, 917–924.

Coleman, M., 2005. Axon degeneration mechanisms: commonality amid diversity. Nat. Rev. Neurosci. 6, 889–898.

Corona, A.W., Huang, Y., O'Connor, J.C., Dantzer, R., Kelley, K.W., Popovich, P.G., Godbout, J.P., 2010. Fractalkine receptor (CX3CR1) deficiency sensitizes mice to the behavioral changes induced by lipopolysaccharide. J. Neuroinflammation 7, 93.

Davalos, D., Grutzendler, J., Yang, G., Kim, J.V., Zuo, Y., Jung, S., Littman, D.R., Dustin, M.L., Gan, W.B., 2005. ATP mediates rapid microglial response to local brain injury in vivo. Nat. Neurosci. 8, 752–758.

David, S., Kroner, A., 2011. Repertoire of microglial and macrophage responses after spinal cord injury. Nat. Rev. Neurosci. 12, 388–399.

Donnelly, D.J., Popovich, P.G., 2008. Inflammation and its role in neuroprotection, axonal regeneration and functional recovery after spinal cord injury. Exp. Neurol. 209, 378–388.

Donnelly, D.J., Longbrake, E.E., Shawler, T.M., Kigerl, K.A., Lai, W., Tovar, C.A., Ransohoff, R.M., Popovich, P.G., 2011. Deficient CX3CR1 signaling promotes recovery after mouse spinal cord injury by limiting the recruitment and activation of Ly6Clo/iNOS+ macrophages. J. Neurosci. Off. J. Soc. Neurosci. 31, 9910–9922.

Dunay, I.R., Damatta, R.A., Fux, B., Presti, R., Greco, S., Colonna, M., Sibley, L.D., 2008. Gr1(+) inflammatory monocytes are required for mucosal resistance to the pathogen Toxoplasma gondii. Immunity 29, 306–317.

Feng, G., Mellor, R.H., Bernstein, M., Keller-Peck, C., Nguyen, Q.T., Wallace, M., Nerbonne, J.M., Lichtman, J.W., Sanes, J.R., 2000. Imaging neuronal subsets in transgenic mice expressing multiple spectral variants of GFP. Neuron 28, 41–51.

Filous, A.R., Evans, T.A., Lang, B.T., Silver, J., 2013. Synaptic-like connections between dystrophic axons and NG2+ cells: another reason for regeneration failure after spinal cord injury. Society for Neuroscience Abstracts. Society for Neuroscience.

Fitch, M.T., Silver, J., 2008. CNS injury, glial scars, and inflammation: inhibitory extracellular matrices and regeneration failure. Exp. Neurol. 209, 294–301.

Gaupp, S., Pitt, D., Kuziel, W.A., Cannella, B., Raine, C.S., 2003. Experimental autoimmune encephalomyelitis (EAE) in CCR2(−/−) mice: susceptibility in multiple strains. Am. J. Pathol. 162, 139–150.

Geissmann, F., Jung, S., Littman, D.R., 2003. Blood monocytes consist of two principal subsets with distinct migratory properties. Immunity 19, 71–82.

Ginhoux, F., Greter, M., Leboeuf, M., Nandi, S., See, P., Gokhan, S., Mehler, M.F., Conway, S.J., Ng, L.G., Stanley, E.R., Samokhvalov, I.M., Merad, M., 2010. Fate mapping analysis reveals that adult microglia derive from primitive macrophages. Science 330, 841–845.

Greer, J.E., Hånell, A., McGinn, M.J., Povlishock, J.T., 2013. Mild traumatic brain injury in the mouse induces axotomy primarily within the axon initial segment. Acta Neuropathol. 126 (1), 59–74.

Hawthorne, A.L., Hu, H., Kundu, B., Steinmetz, M.P., Wylie, C.J., Deneris, E.S., Silver, J., 2011. The unusual response of serotonergic neurons after CNS injury: lack of axonal dieback and enhanced sprouting within the inhibitory environment of the glial scar. J. Neurosci. Off. J. Soc. Neurosci. 31, 5605–5616.

Horn, K.P., Busch, S.A., Hawthorne, A.L., van Rooijen, N., Silver, J., 2008. Another barrier to regeneration in the CNS: activated macrophages induce extensive retraction of dystrophic axons through direct physical interactions. J. Neurosci. 28, 9330–9341.

Hsu, J.Y., McKeon, R., Goussev, S., Werb, Z., Lee, J.U., Trivedi, A., Noble-Haeusslein, L.J., 2006. Matrix metalloproteinase-2 facilitates wound healing events that promote functional recovery after spinal cord injury. J. Neurosci. 26, 9841–9850.

Huang, D., Shi, F.D., Jung, S., Pien, G.C., Wang, J., Salazar-Mather, T.P., He, T.T., Weaver, J.T., Ljunggren, H.G., Biron, C.A., Littman, D.R., Ransohoff, R.M., 2006. The neuronal chemokine CX3CL1/fractalkine selectively recruits NK cells that modify experimental autoimmune encephalomyelitis within the central nervous system. FASEB J. 20, 896–905.

Jung, S., Aliberti, J., Graemmel, P., Sunshine, M.J., Kreutzberg, G.W., Sher, A., Littman, D.R., 2000. Analysis of fractalkine receptor CX(3)CR1 function by targeted deletion and green fluorescent protein reporter gene insertion. Mol. Cell. Biol. 20, 4106–4114.

Kerschensteiner, M., Schwab, M.E., Lichtman, J.W., Misgeld, T., 2005. In vivo imaging of axonal degeneration and regeneration in the injured spinal cord. Nat. Med. 11, 572–577.

Kierdorf, K., Katzmarski, N., Haas, C.A., Prinz, M., 2013a. Bone marrow cell recruitment to the brain in the absence of irradiation or parabiosis bias. PLoS One 8, e58544.

Kierdorf, K., et al., 2013b. Microglia emerge from erythromyeloid precursors via Pu.1- and Irf8-dependent pathways. Nat. Neurosci. 16, 273–280.

Kigerl, K.A., Gensel, J.C., Ankeny, D.P., Alexander, J.K., Donnelly, D.J., Popovich, P.G., 2009. Identification of two distinct macrophage subsets with divergent effects causing either neurotoxicity or regeneration in the injured mouse spinal cord. J. Neurosci. Off. J. Soc. Neurosci. 29, 13435–13444.

Lee, S., Varvel, N.H., Konerth, M.E., Xu, G., Cardona, A.E., Ransohoff, R.M., Lamb, B.T., 2010. CX3CR1 deficiency alters microglial activation and reduces beta-amyloid deposition in two Alzheimer's disease mouse models. Am. J. Pathol. 177, 2549–2562.

Li, E., Noda, M., Doi, Y., Parajuli, B., Kawanokuchi, J., Sonobe, Y., Takeuchi, H., Mizuno, T., Suzumura, A., 2012. The neuroprotective effects of milk fat globule-EGF factor 8 against oligomeric amyloid β toxicity. J. Neuroinflammation 9, 148.

Ma, M., Wei, T., Boring, L., Charo, I.F., Ransohoff, R.M., Jakeman, L.B., 2002. Monocyte recruitment and myelin removal are delayed following spinal cord injury in mice with CCR2 chemokine receptor deletion. J. Neurosci. Res. 68, 691–702.

Mahad, D., Callahan, M.K., Williams, K.A., Ubogu, E.E., Kivisäkk, P., Tucky, B., Kidd, G., Kingsbury, G.A., Chang, A., Fox, R.J., Mack, M., Sniderman, M.B., Ravid, R., Staugaitis, S.M., Stins, M.F., Ransohoff, R.M., 2006. Modulating CCR2 and CCL2 at the blood–brain barrier: relevance for multiple sclerosis pathogenesis. Brain 129, 212–223.

Matsumoto, Y., Fujiwara, M., 1987. Absence of donor-type major histocompatibility complex class I antigen-bearing microglia in the rat central nervous system of radiation bone marrow chimeras. J. Neuroimmunol. 17, 71–82.

Mawhinney, L.A., Thawer, S.G., Lu, W.Y., Rooijen, N., Weaver, L.C., Brown, A., Dekaban, G.A., 2012. Differential detection and distribution of microglial and hematogenous macrophage populations in the injured spinal cord of lys-EGFP-ki transgenic mice. J. Neuropathol. Exp. Neurol. 71, 180–197.

McPhail, L.T., Stirling, D.P., Tetzlaff, W., Kwiecien, J.M., Ramer, M.S., 2004. The contribution of activated phagocytes and myelin degeneration to axonal retraction/dieback following spinal cord injury. Eur J Neurosci 20, 1984–1994.

Nijagal, A., Le, T., Wegorzewska, M., Mackenzie, T.C., 2011. A mouse model of in utero transplantation. J. Vis. Exp. 47, e2303.

Nimmerjahn, A., Kirchhoff, F., Helmchen, F., 2005. Resting microglial cells are highly dynamic surveillants of brain parenchyma in vivo. Science 308, 1314–1318.

Oshima, T., Sonoda, K.H., Tsutsumi-Miyahara, C., Qiao, H., Hisatomi, T., Nakao, S., Hamano, S., Egashira, K., Charo, I.F., Ishibashi, T., 2006. Analysis of corneal inflammation induced by cauterisation in CCR2 and MCP-1 knockout mice. Br. J. Ophthalmol. 90, 218–222.

Popovich, P.G., Hickey, W.F., 2001. Bone marrow chimeric rats reveal the unique distribution of resident and recruited macrophages in the contused rat spinal cord. J. Neuropathol. Exp. Neurol. 60, 676–685.

Popovich, P.G., Guan, Z., Wei, P., Huitinga, I., van Rooijen, N., Stokes, B.T., 1999. Depletion of hematogenous macrophages promotes partial hindlimb recovery and neuroanatomical repair after experimental spinal cord injury. Exp. Neurol. 158, 351–365.

Popovich, P.G., van Rooijen, N., Hickey, W.F., Preidis, G., McGaughy, V., 2003. Hematogenous macrophages express CD8 and distribute to regions of lesion cavitation after spinal cord injury. Exp. Neurol. 182, 275–287.

Powers, B.E., Lasiene, J., Plemel, J.R., Shupe, L., Perlmutter, S.I., Tetzlaff, W., Horner, P.J., 2012. Axonal thinning and extensive remyelination without chronic demyelination in spinal injured rats. J. Neurosci. 32, 5120–5125.

Saederup, N., Cardona, A.E., Croft, K., Mizutani, M., Cotleur, A.C., Tsou, C.L., Ransohoff, R.M., Charo, I.F., 2010. Selective chemokine receptor usage by central nervous system myeloid cells in CCR2-red fluorescent protein knock-in mice. PLoS One 5, e13693.

Schafer, D.P., Lehrman, E.K., Kautzman, A.G., Koyama, R., Mardinly, A.R., Yamasaki, R., Ransohoff, R.M., Greenberg, M.E., Barres, B.A., Stevens, B., 2012. Microglia sculpt postnatal neural circuits in an activity and complement-dependent manner. Neuron 74, 691–705.

Schafer, D.P., Lehrman, E.K., Stevens, B., 2013. The "quad-partite" synapse: Microglia-synapse interactions in the developing and mature CNS. Glia 61, 24–36.

Schwartz, M., Yoles, E., 2006. Immune-based therapy for spinal cord repair: autologous macrophages and beyond. J. Neurotrauma 23, 360–370.

Shechter, R., London, A., Varol, C., Raposo, C., Cusimano, M., Yovel, G., Rolls, A., Mack, M., Pluchino, S., Martino, G., Jung, S., Schwartz, M., 2009. Infiltrating blood-derived macrophages are vital cells playing an anti-inflammatory role in recovery from spinal cord injury in mice. PLoS Med. 6, e1000113.

Shechter, R., Miller, O., Yovel, G., Rosenzweig, N., London, A., Ruckh, J., Kim, K.W., Klein, E., Kalchenko, V., Bendel, P., Lira, S.A., Jung, S., Schwartz, M., 2013. Recruitment of beneficial M2 macrophages to injured spinal cord is orchestrated by remote brain choroid plexus. Immunity 38, 555–569.

Shen, Y., Tenney, A.P., Busch, S.A., Horn, K.P., Cuascut, F.X., Liu, K., He, Z., Silver, J., Flanagan, J.G., 2009. PTPsigma is a receptor for chondroitin sulfate proteoglycan, an inhibitor of neural regeneration. Science 326, 592–596.

Stirling, D.P., Yong, V.W., 2008. Dynamics of the inflammatory response after murine spinal cord injury revealed by flow cytometry. J. Neurosci. Res. 86, 1944–1958.

Takeshita, Y., Ransohoff, R.M., 2012. Inflammatory cell trafficking across the blood–brain barrier: chemokine regulation and in vitro models. Immunol. Rev. 248, 228–239.

Titsworth, W.L., Liu, N.K., Xu, X.M., 2008. Role of secretory phospholipase a(2) in CNS inflammation: implications in traumatic spinal cord injury. CNS Neurol. Disord. Drug Targets 7, 254–269.

Van Rooijen, N., Sanders, A., 1994. Liposome mediated depletion of macrophages: mechanism of action, preparation of liposomes and applications. J. Immunol. Methods 174, 83–93.

Yona, S., Kim, K.W., Wolf, Y., Mildner, A., Varol, D., Breker, M., Strauss-Ayali, D., Viukov, S., Guilliams, M., Misharin, A., Hume, D.A., Perlman, H., Malissen, B., Zelzer, E., Jung, S., 2013. Fate mapping reveals origins and dynamics of monocytes and tissue macrophages under homeostasis. Immunity 38, 79–91.